Journal of Structural Geology, Vol. 12, No. 2, pp. 227 to 241, 1990
Printed in Great Britain

0191-8141/90 $03.00+0.00

The evolution of mesoscopic imbricate thrust faults—an example from the Vermont Foreland, U.S.A.

ROLFE S. STANLEY

Department of Geology, University of Vermont, Burlington, VT 05405, U.S.A.

(*Received* 23 *January* 1989; *accepted in revised form* 17 *August* 1989)

Abstract—An outcrop of a thin (30 cm) bed of micrite surrounded by thicker sequences of well-cleaved, calcareous shale in the Ordovician flysch of western Vermont records a complex history of imbricate faulting and associated folding. The calcareous shale has been shortened by pressure solution. Cross-cutting relations among the floor, ramp and roof faults indicate that faulting progressed from the hinterland (east) to the foreland (west). All the ramp faults developed from arrays of W-climbing en échelon extension fractures. All other faults were controlled by the weaker bedding planes that surround the micrite, and are found at various levels in the shale. Each fault is marked by layers of highly twinned, sparry calcite and black carbonaceous shale selvedge. Simple shear along the floor thrust has rotated the S_1 cleavage toward the foreland and produced, along with volume change, a pressure-solution cleavage in the fault zone. All cleavages have progressively developed from the hinterland to the foreland during folding and faulting of the micrite. Layer-parallel shortening measured in both rock types is between 11 and 16%.

INTRODUCTION

THE geometry of foreland deformation has been the subject of a number of important papers during the last 10 years (Gwinn 1970, Boyer & Elliot 1982, Suppe 1982, 1985, Ramsay & Huber 1987, to cite a few). Data constraining foreland geometry are based on standard geological mapping, hydrocarbon drilling and seismic reflection studies. The conclusions and inferences resulting from this information, however, are often speculative because the geometric interpretations are not unique. On the other hand, the value of outcrop-scale (mesoscopic) structures in understanding foreland deformation has been demonstrated by Serra (1977), Bosworth (1984) and Nickelson (1986). Because the geometry is fully exposed, one can concentrate on process and evolution without being hampered by the uncertainties characteristic of regional studies. Care must be taken, however, when the conclusions on mechanisms and process are extrapolated to larger structures because of the scale change.

This paper discusses the mechanisms and evolution of a series of imbricate thrust faults that are present in the Cumberland Head Formation of Middle Ordovician age in the foreland of western Vermont (Fig. 1). The outcrop is located 8 km west of the Champlain thrust fault, approximately 1400 m below the restored westward projection of the thrust surface, assuming that the dip of 10–15° in outcrop was constant. Major displacement on the thrust occurred during the Middle Ordovician Taconian orogeny and is estimated to be in the order of 35–80 km (Rowley 1982, Stanley & Ratcliffe 1985).

The following major questions need to be discussed. (1) How do ramp faults form? (2) Are there criteria for determining whether imbricate thrust faults propagate toward the foreland or hinterland? (3) What is the relation between faulting and cleavage development? (4) What processes are involved in the formation of fault zones? (5) Are there criteria that indicate the relative importance of each fault? (6) What is the integrated evolution of the fractures, faults and associated cleavage? The first five questions will be largely addressed by direct evidence at the outcrop. The last question will be answered by palinspastically restoring the imbricated and cleaved sequence to its undeformed state. A discussion of pore pressure and deformation rates will follow. The conclusions from this study can only be confidently applied to other foreland settings where the rock sequence and composition are similar. Many of the processes, however, may apply to other foreland sequence irrespective of the size of the structure.

THE OUTCROP

Five imbricate thrust faults and associated ramps are exposed in a 30 cm thick bed of micrite that extends 14 m along an azimuth of N80°E (Fig. 2). Three of the imbricate faults form a central duplex that is separated from two simple ramps at either end of the outcrop by approximately 2.5 m of flats. The micrite bed is surrounded by at least 1.5 m of well-cleaved calcareous shale. Bedding-plane faults are present along the upper and lower surfaces of the micrite where they merge with ramp faults that cut across the micrite bed at an angle of approximately 30°. The lower bedding-plane fault or floor thrust is relatively planar and the fault zone is thick compared to the upper bedding-plane faults. The latter are folded in the ramp areas, cut by ramp faults and the fault zones are thin. Along the intervening flats the upper faults are generally planar and cut in many places by the S_1 cleavage. The lower bedding-plane fault is the major décollement across the outcrop. Older bedding-

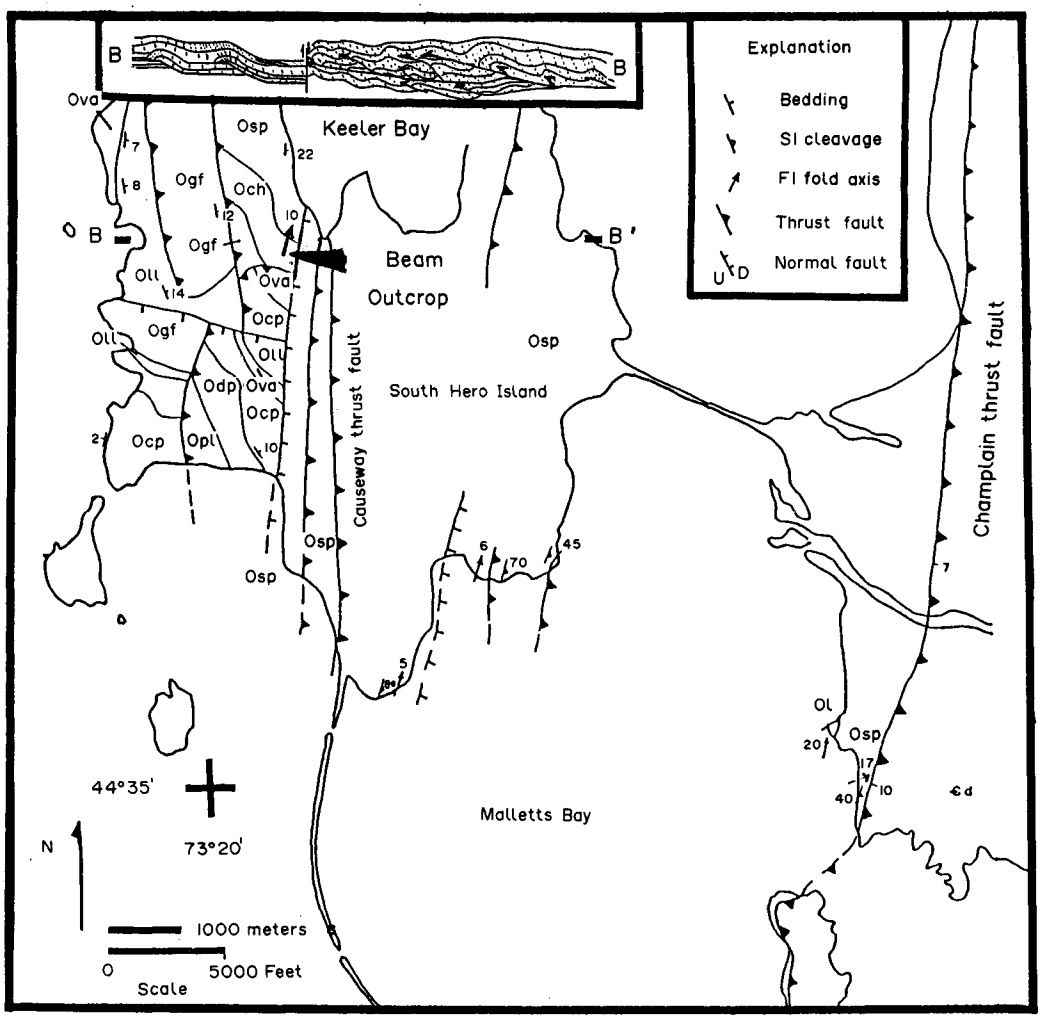

Fig. 1. Geological map of the southern part of South Hero Island, Vermont, U.S.A. The outcrop is located in the Cumberland Head Formation (Och) on the east side of U.S. Route 2 just southwest of Keeler Bay (see arrow). The trace of the Champlain thrust fault, which places Lower Cambrian Dunham Dolomite (Cd) over the Middle Ordovician Stony Point Shale (Osp), is located along the eastern part of the map. The stratigraphic units are largely Ordovician limestones and shales and their identity is not pertinent to this study. Cross-section B–B' is drawn through the latitude of the 'beam' outcrop. For further information see the Geological Map of Vermont (Doll *et al.* 1961). Geological map and cross-section were done by Leonard (1985).

plane faults are also present throughout the shale where they are offset by the penetrative S_1 cleavage.

All the fault surfaces are covered by layers of sparry calcite that vary in thickness from several mm to 10 cm (Fig. 3a). In all but the thinnest layers, the calcite is arranged in distinct layers that are separated by discontinuous selvedge of dark gray shale. Each of the layers are marked by grooves or slickenlines that trend N56°W and are essentially parallel from layer to layer (Fig. 2b). In sections oriented perpendicular to the layering and parallel to the slickenlines the shale selvedges are more parallel to each other than in sections cut perpendicular to the slickenlines where the selvedges either anastomose or conform to the cross-section of the grooves (Figs. 3b & c). In the parallel sections, however, some of the selvedge layers are truncated by more continuous surfaces. One of these can be traced for 1.5 m or more along the floor thrust. At a number of places along the different fault zones small dikes of sparry calcite have intruded the lower part of the calcite–shale layers. The fault-zone fabrics are most clearly displayed along the floor thrust where the calcite–selvedge layers are more abundant.

Fractures are common throughout the micrite bed where they are oriented at either a high angle or low angle to the bedding. Most fractures are filled with sparry calcite. The most prominent fractures are arranged in en échelon arrays that climb either to the west or the east (Fig. 4). Most of these arrays are located in ramp areas. Others are present in the flat regions of the micrite bed or along the W-facing limb of a small flexure. A few are present in the flat regions of the bed. The fractures in many of the arrays in the ramp regions are folded and some are cut by younger generations of en échelon fractures (Fig. 4c). In the eastern ramp (Fig. 2) the hangingwall and footwall are cut by near-vertical clastic dikes that are filled with fragments of the surrounding micrite embedded in sparry calcite (Fig. 4d).

Two well developed pressure-solution cleavages are present throughout the calcareous shale. The first and most conspicuous one, S_1, has an averaged strike of N20°E and dip of 60°E (Figs. 2b and 4a) although the

strike does vary more than the dip. S_1 surfaces are covered by a black, carbon-rich, illite and kaolinite selvedge which is less than 0.5 cm thick. Although many of the cleavage surfaces are vertically continuous through the shale, some of them are short and discontinuous with tapered ends. The thickest selvedge occurs on the most continuous surfaces. The surfaces of the selvedge are not lineated although some are polished. The S_1 cleavage offsets bedding and the older bedding-plane thrust faults with a down-to-the-east sense throughout much of the outcrop. This displacement is greatest where a selvedge is the thickest and it gradually is reduced to zero as a selvedge thins towards the tapered ends of the shorter cleavage surfaces. The average width of the microlithons between the S_1 surfaces is 5.6 cm. The S_1 cleavage not only cuts the older bedding-plane faults but cuts across most of the roof faults on top of the micrite bed.

A second, well developed cleavage, S_t, is restricted to a 30 cm thick zone directly below the floor thrust (Figs.

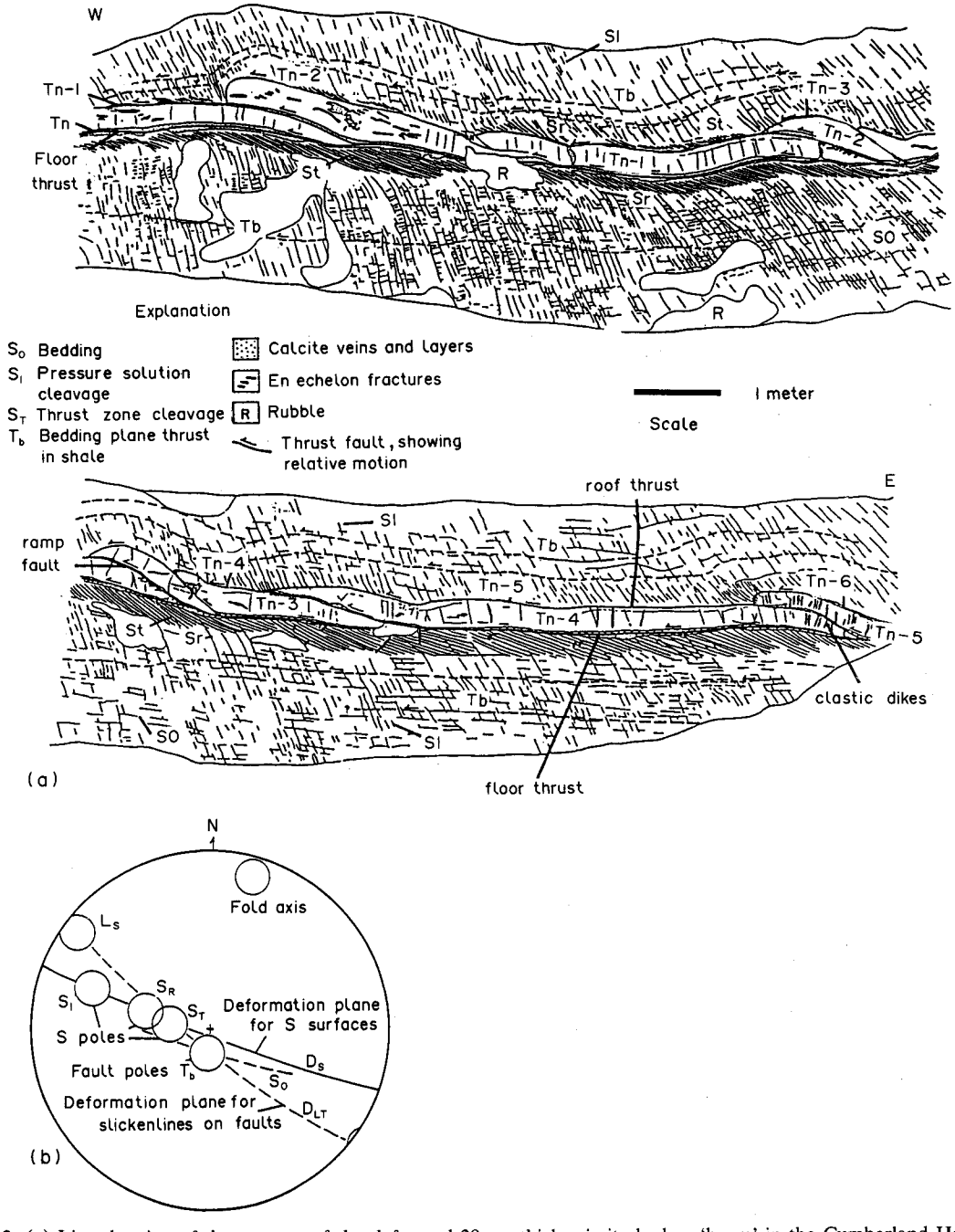

Fig. 2. (a) Line drawing of the outcrop of the deformed 30 cm thick micrite bed or 'beam' in the Cumberland Head Formation. The drawing, which is split into two parts, was traced from a photomosaic of the outcrop. The central duplex is located on the east end of the upper drawing and it is repeated on the west end of the lower drawing. The relative age of the faults is indicated by the symbols T_n, T_{n-1}, . . ., etc., where T_{n-1} is older than T_n. The letter n represents an unknown number. The dash is a minus sign. S_r refers to the rotated S_1 cleavage near the micrite bed. (b) Lower-hemisphere, equal-area net projection showing the dominant position of the major structural elements at the 'beam outcrop'. The structural elements are identified in (a). *Ls* refers to the dominant orientation of slickenlines on the thrust faults. The slickenlines on the older thrust faults are rotated along the deformation plane for slickenlines. The fold axis trends N15°E and plunges 10°.

3a and 4a). The individual cleavage surfaces are thinner (about 1 mm thick), more closely spaced (about 1 cm or more) and are covered with a thin selvedge (less than 1 mm). Furthermore, S_t dips to the east at only 6° compared to the steeper dip of S_1 (Fig. 2b). S_t is also developed along the roof thrust of the micrite bed, but the zone is thinner and it is more difficult to recognize because the roof faults have been folded in the ramp areas and deformed by S_1. The S_t cleavage is definitely related to movement of the thrust faults because it is only found near the faults.

In the zone near the floor thrust and the roof faults the S_1 cleavage is rotated eastward so that the steeper 60° dip in the shale is reduced to 25° (Figs. 2b and 4a). The strike of the rotated S_1 (hereafter referred to as S_r) is the same as S_1 away from the faults. The rotation of S_1 through an angle of 35° indicates that movement on the décollement was east-over-west in the direction N56°W as indicated by the slickenlines. This sense of displacement is consistent with the orientation of S_t since the normal to S_t would correspond to the direction of maximum finite compressive strain.

Cleavage, similar to S_1 and S_t, is totally absent from the micrite bed. In a few places, however, a very thin (less than 1 mm), stylolitic to very irregular cleavage is oriented perpendicular to bedding in the micrite (Fig. 4b). Where it is formed, the cleavage surfaces are separated from each other by at least 6–10 cm. The form, orientation and limited distribution of this cleavage indicates that it formed very early in the deformation sequence while compression was essentially parallel to the micrite bed.

RAMP FAULTS

All the E-dipping ramp faults develop from arrays of W-climbing, en échelon fractures. The individual extension fractures within the arrays dip 7–11° more steeply to the west than bedding in the flats or on the western limb of a gentle, asymmetrical fold (Fig. 4a). The development of these faults is well preserved in the ramp regions where the en échelon arrays are folded or cut by continuous ramp faults. After a new array formed, distributed shear strain along the W-climbing array rotated the older parts of the extension fractures while their tips continue to grow in the direction of σ_1 resulting in the S-shaped pattern (Fig. 4c). Shear strains along these arrays are in the order of 1.4 (angular shear strain of 54°) calculated using equation (2.3) of Ramsay & Huber (1983), and indicate that at least 5.6 cm of displacement occurred across the arrays before they failed as a ramp fault. Before failure, the plane of the array was weakened as new arrays of planar fractures were superposed over the older arrays. These fractures eventually coalesced and developed into ramp faults (Fig. 3). The presence of sparry calcite and cavities in the fractures indicates that the fractures opened rapidly (Figs. 4b & c).

East-climbing, en échelon fracture arrays are also present in the micrite bed where they are concentrated in the ramp regions (Fig. 4c). The individual extension fractures in the E-climbing arrays are either parallel to or dip more steeply E than bedding. These angular relations are important because they indicate that the E-climbing arrays were not formed at the same time as the W-climbing arrays because their respective fractures are not parallel. Although some of the fractures in the E-climbing arrays are deformed into Z shapes, none of the arrays developed into backthrusts. Calculated shear strains along these arrays give a maximum value of 1.1 (47°). I suggest that they formed as a result of continued compression after the ramp faults were locally locked and before failure developed in another ramp zone farther to the west.

The orientation of the extension fractures in the micrite bed are important because they indicate the orientation of the bedding relative to the direction of maximum compressive stress (σ_1), which was essentially horizontal during deformation. During the early stage of deformation, bedding was essentially parallel to σ_1 because the styolitic cleavage, which forms perpendicular to σ_1, is perpendicular to bedding (Fig. 4b). The bedding was then rotated eastward relative to the direction of σ_1 so that the individual extension fractures in the W-climbing arrays could form at a more westerly inclined angle than bedding (Fig. 4b). East-over-west displacement on bedding plane faults could occur at this time because the shear stress was now high enough to overcome frictional resistance. Continued compression across the micrite bed resulted in very minor, E-directed movement along the E-climbing arrays. The orientation of these later extension fractures was then controlled by the local orientation of σ_1 in the ramp regions.

FAULT CHRONOLOGY

The bedding plane faults in the surrounding shales are clearly older than the faults in the micrite bed because

Fig. 3. (a) The central duplex showing two imbricate thrust faults (Fig. 2). The eastern ramp (ER) and central roof thrust (CRT) are cut by the western ramp fault (WR). En échelon extension fractures (F) of an early W-climbing array are rotated counterclockwise along the footwall block of the ramp fault. The S_1 cleavage is rotated (S_r) westward in the shale directly below the floor thrust (FT). The thinly-spaced, thrust-zone cleavage (S_t) cuts the rotated S_1 and dips gently to the east below the floor thrust. (b) A 10 cm fault zone (FZ) along the floor thrust. The view is oriented perpendicular to the slickenlines and shows the anastomosing layers of sparry calcite and black shale selvedge. (c) A view of the same fault zone oriented parallel to the slickenline direction, showing black shale selvedges (S) between layers of sparry calcite. (d) Negative photomicrograph of a thin section of the fault zone cut parallel to the slickenline direction showing layers of twinned calcite (grey color) and black selvedge of shale (white color). These layers define slip surfaces that were active during the history of the fault zone. The stair-step selvedge above and to the left of 'S' indicates left-lateral (east-over-west) shear which is consistent with the E-dipping S_t cleavage marked by fine dark lines in the lower part of the photograph.

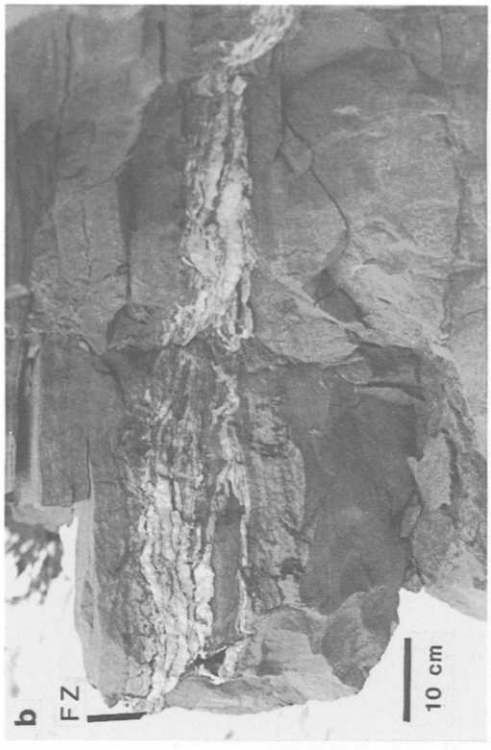
b
FZ
10 cm

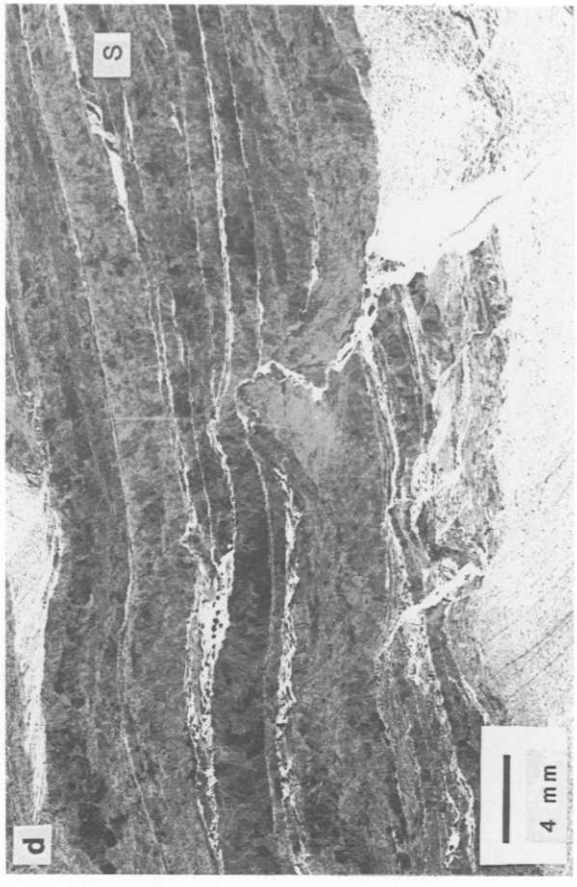
d
S
4 mm

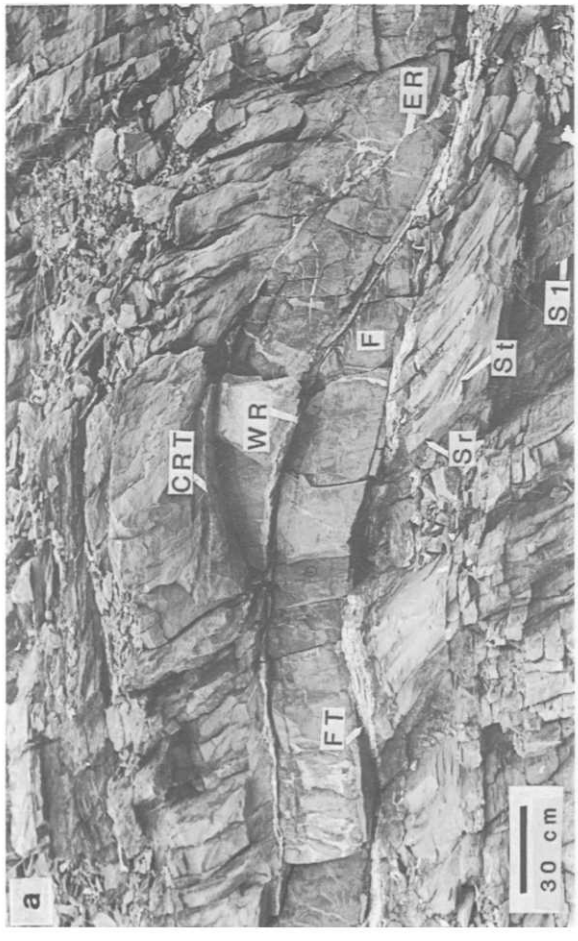
a
CRT
WR
FT
F
ER
St
Sr
S1
30 cm


c
Sr
5 cm

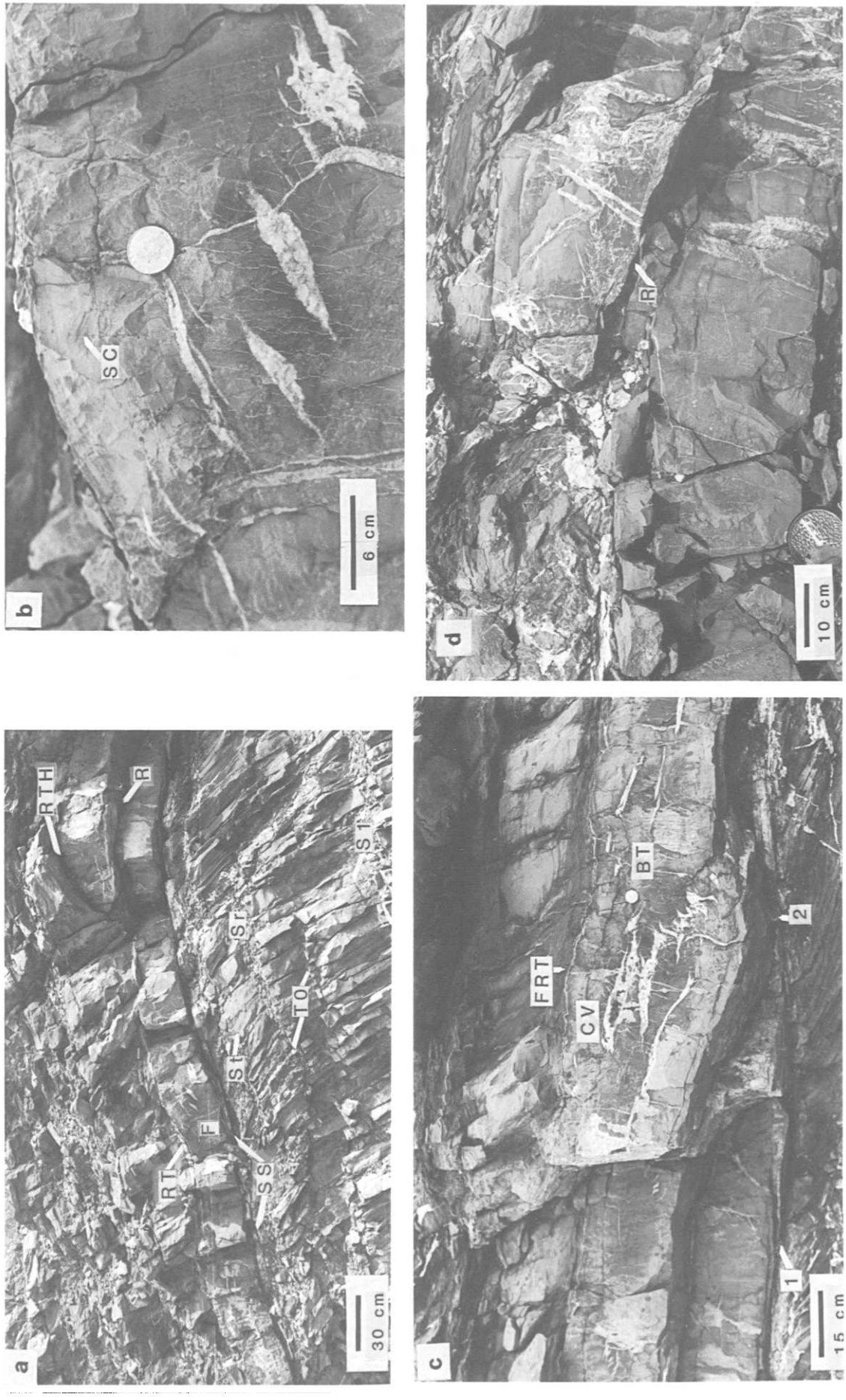
a
RTH
R
RT
F
St
Sr
SS
TO
S1
30 cm
b
SC
6 cm
c
FRT
CV
BT
1
2
15 cm
d
R
10 cm

they are cut and offset by the S_1 cleavage. Although the bedding-plane faults that are in direct contact with the micrite bed may have formed originally at this time there is abundant evidence that they were active long after those in the shale. Their average age therefore is younger. Furthermore, they play an essential role in the development of the ramp faults.

The evidence for the relative age of each of the faults is found in the regions where the ramp faults merge with the roof and floor faults. For example, in the western part of Fig. 2 (see also Fig. 4a) the ramp fault (T_{n-1}) cuts across the upper bedding-plane fault (T_{n-2}) of the hangingwall block but merges asymptotically with the floor fault (T_n) of the footwall block. Furthermore, the roof fault of the hangingwall block is folded and cut by S_1 cleavage. At the junction of the ramp fault and the floor fault, the quasiplanar slip surfaces in the calcite–shale fault zone cut across the fault zone of the ramp fault. The relative age relations therefore are clear—the oldest fault of the three is the roof thrust and is designated T_{n-2}. The youngest fault is the floor thrust (T_n). This same relative chronology applies to all the ramps and duplexes to the east (Figs. 3a and 4c).

Several important conclusions result from this analysis. First, the imbricate faults that comprise the roof, ramp and floor fault system become younger to the west or towards the foreland for the Northern Appalachians. This conclusion is based on direct evidence and not on an assumption about the fault sequence. Second, the floor fault was continually reactivated during the evolution of the fault system, becoming younger to the west and developing into the most continuous fault in the outcrop. This second conclusion explains why the fault zone for the floor fault is thicker than the fault zones along the ramp or roof faults (Fig. 3a).

The geometry of the westward-younging faults in the micrite bed represents the standard 'piggyback' sequence described for many mountain chains in which the thrust faults become younger toward the foreland (Boyer & Elliot 1982, for example). Imbricate faults that become younger toward the hinterland would have a quite different geometry and cross-cutting sequence (Fig. 5). Here the roof fault can take on various configurations as irregularities caused by earlier ramp anticlines are eliminated by continued movement on the roof fault zone (Figs. 5b–d). Ramps and duplexes with this geometry have not been recognized in the shales of western Vermont.

FAULT-ZONE DEPOSITS

The floor fault has been active throughout the development of the imbricate system and should record the most complete history, particularly at its eastern end. The fabric of sparry calcite and shale selvedges along the floor fault, however, appears to be equally complex at both ends. No fabric elements can be correlated with age because other factors such as fault junctions in the ramp areas and broad flexures along the intervening flats control the thickness and complexity of the fault zone (Fig. 3a).

Leonard (1985) studied the fault zones in the field and in oriented thin sections cut parallel and perpendicular to the slickenlines and found that the following relations are important in understanding the evolution of the fault-zones.

(1) All the fault zones are filled with veins of sparry calcite and minor quartz which are generally oriented either parallel or at a low angle to the fault surface (Figs. 3b–d). Vertical veins, which commonly join sills higher in the fault zone, are more common in the lowest layers of the fault zone and in the shale directly beneath the fault zone.

(2) Discontinuous, dark, stylolitic clay laminae with concentrations of quartz adjacent to or within the laminae are interlayered with the calcite in all but the thinnest zones. The laminae are identical in appearance to the selvedges on the S_1 cleavage surfaces. Some of the clay laminae are continuous with shale chips which preserve varying degrees of pressure solution (Fig. 3d).

(3) The size of the sparry calcite is directly proportional to vein width. Most grains are bladed in form, but their long axis is not preferentially aligned. The calcite in all the layers is twinned with the greatest density occurring in the thinner layers between shale laminae where the grains are turbid and small (Fig. 3d).

Fig. 4. (a) Imbricate thrust in the micrite beam at the west end of the outcrop showing a ramp fault (R) cutting a roof thrust of the hangingwall block (RTH). To the west the ramp fault becomes the roof thrust (RT) of the footwall block. The thrust is marked by a thin layer of calcite with shale selvedge. The floor thrust contains a planar slip surface (SS). A W-climbing array of undeformed en échelon fractures (F) is present in the west limb of a very gentle fold in the micrite bed. The individual fractures dip more steeply to the west than the bedding in the micrite bed. Below the micrite bed the S_1 cleavage is rotated westward as it (S_r) approaches the floor thrust. In the 30 cm thick zone beneath the thrust a closely-spaced, unrotated cleavage (S_t) cuts the older S_1 cleavage. Both S_1 and S_t indicate westward movement of the beam along the floor thrust. Older bedding plane thrusts (T_0) in the shale are offset by S_1. (b) En échelon extension fractures with sparry calcite in a W-climbing array. An early stylolitic cleavage (SC) above the coin is oriented perpendicular to the bedding. (c) Deformed S-shaped extension fractures in a W-climbing array located in the hangingwall block (upper right) at the west end of the outcrop. Several younger undeformed fractures cut the older S-shaped fractures. A 20 cm long undeformed fracture has a central vug (CV) with calcite and quartz crystals. The coin is located over an E-climbing array that marks the backthrust position (BT). A folded roof thrust (FRT) on the eastern hangingwall block above the en échelon fractures is marked by a thin layer of calcite and shale selvedge with slickenlines. The planar slip surface in the lower floor thrust (point 1 in photograph) directly below the micrite bed truncates the ramp fault at point 2. The junction of the two faults is filled with a thick wedge of calcite. (d) Ramp thrust (R) at the east end of the outcrop showing dikes of calcite with shale chips cutting the hangingwall and footwall blocks. A W-climbing array of en échelon fractures in the hangingwall block is parallel to the ramp fault. The numerous cleavage planes at the nose of the hangingwall block suggests that it was an area of high differential stress where pressure solution was extensive.

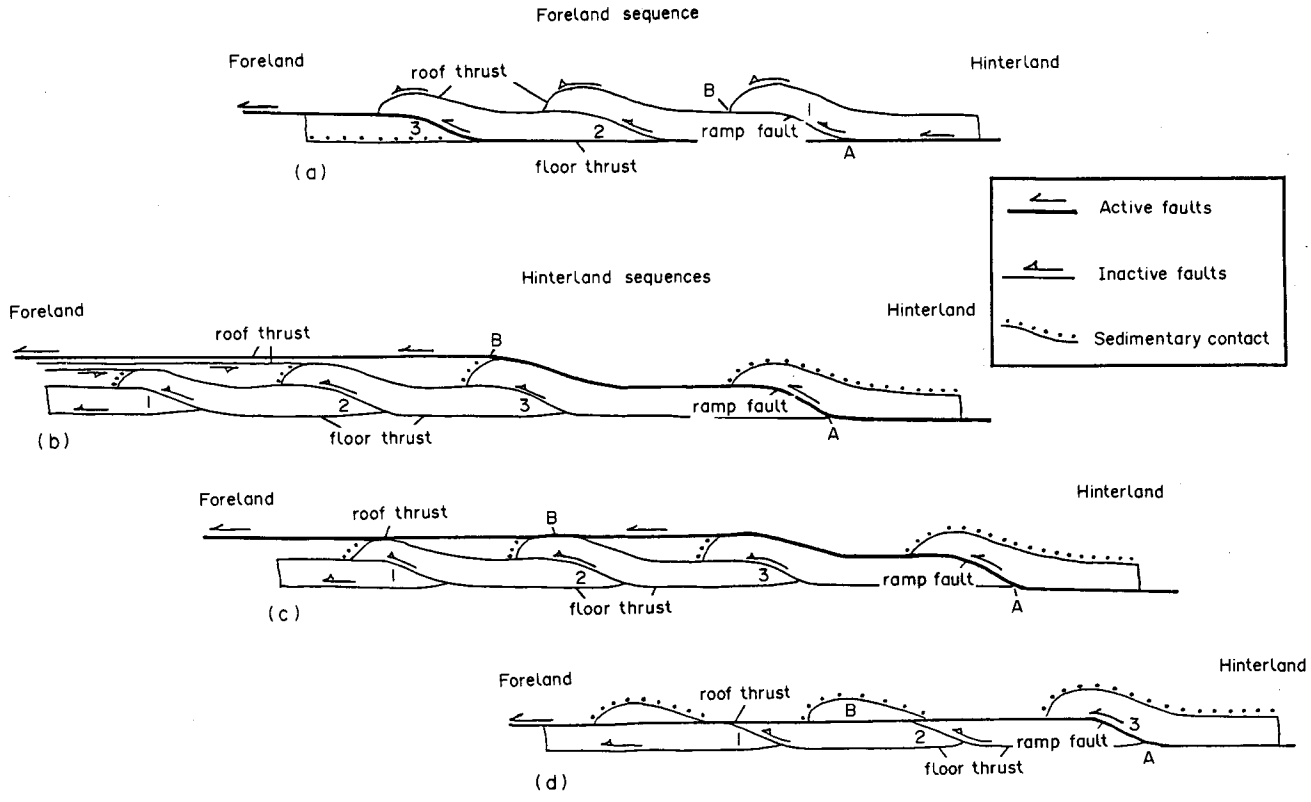

Fig. 5. Comparison between imbricate thrust faults that become younger toward the foreland (foreland sequence) and those that become younger toward the hinterland (hinterland sequence). In all models the ramp faults are numbered 1, 2 and 3 in the direction of the ramp with the youngest age. In (a) the foreland sequence, the older roof thrusts are cut by the younger ramp faults (location B) whereas the ramp faults are cut by the floor thrust nearest the foreland (location A). The age and the fault-zone fabrics along the floor thrust become older and more complex toward the hinterland. In the hinterland sequences each floor thrust toward the foreland is cut by the ramp fault with the next higher number toward the hinterland (location A, for example). The roof thrusts must cut across folded bedding (not shown) along the limb facing the foreland (location B) in (b) and (c). (d) is considered an unlikely possibility in nature because the roof thrust must cut across the strong rocks of the 'beam' rather than follow the weak layer between the 'beam' and the overlying shale. In all hinterland sequences the age and fault-zone fabrics along the roof thrust become older and more complex toward the foreland. In (b) the number of roof thrusts increases toward the foreland. Their individual fault fabrics may be relatively simple since they may not be involved with repeated movement during each imbrication. The position of the sedimentary contacts, here defined as a contact that is not involved with shortening of the 'beam', is an important criterion that separates foreland from hinterland sequences. In the hinterland sequences either the anticlinal limb facing the foreland (b and c) or the full ramp anticline (d) are sedimentary contacts. In the foreland sequence the ramp thrust caps all the anticlines. A basic assumption in all these models is that faults that have undergone repeated movement during their evolution will be planar or geometrically simple. These faults are labelled the 'active faults' in the models.

(4) The slickenlines on each of the vein layers are formed by grooves rather than calcite fibers (Fig. 3b).

Based on the foregoing information, calcite was deposited along the faults after the initial cohesion was broken along the shale–shale or shale–micrite contacts where the strength contrast is great and the cohesive strength is small. Subsequent failure occurred along the calcite–shale interface and resulted in scabs and chips of the shale being incorporated into the fault zone. During renewed movement the calcite and quartz were dissolved from the shale fragments to form the black selvedges which are interlayered with the calcite and decorate the slip surfaces. As the fault zone thickened, movement could then occur along planar slip surfaces which smoothed out the irregular geometry formed by ramp zones and broad folds. Movement therefore was no longer restricted to the calcite–shale boundaries of thin fault zones, but could occur along any calcite–selvedge boundary that was favorably situated. The resulting clay selvedge then acted as a catalyst that facilitated solution of calcite from the selvedge–calcite boundary of the surrounding veins. Preferential solution in the direction of fault movement produced the slickenline grooves.

Because the floor fault was continually active during the evolution of the imbricate system, it is not surprising to find numerous cross-cutting veins in the thick fault zone deposit. During each of these events the influx of fluid and the subsequent crystallization were rapid enough to form sparry calcite rather than fibered calcite. As the fault zone thickened with layers of calcite and clay selvedge, new veins could form along any surface of weakness within the fault zone rather than being confined to the outer borders with the country rock. With continued movement across the fault zone, the calcite in the older veins became heavily twinned and severely strained.

The fault zone fabrics therefore suggest that fault movement was intermittent, with each event occurring rapidly. During the intervening time, when deformation was slower, pressure solution and calcite twinning may have occurred.

SHORTENING AND CLEAVAGE DEVELOPMENT

Layer-parallel shortening can be calculated from the folds in the ramp areas and structural overlap across the faults. The displacement on faults in the micrite bed ranges from 7.6 to 48.3 cm and totals 134 cm (1.34 m) over a present horizontal distance of 10.7 m. The five anticlines over ramps and the broad folds along the flats account for approximately 12.7 cm of additional shortening so that the total shortening equal 146.7 cm (1.47 m). Total shortening was 13.7% of which folding only accounts for 8.7% of the total reduction in length.

In the shale the corresponding shortening is provided by volume reduction across the cleavage surfaces, S_1 and to a far lesser degree S_t. It is clear that these cleavages formed by pressure solution because they are marked by insoluble residue. Furthermore the abundance of calcite and minor quartz in fractures and along the faults indicates that these two minerals were dissolved from the calcareous shale and deposited in nearby openings. To compare shortening in the micrite bed and the shale, an independent estimate was made for the shale by determining the percentage of insoluble material. Samples of suitable material from four different microlithons were dissolved in hydrochloric acid. The final average residue was 36% of the original volume (a range of 32–39% for four samples). The number of cleavage selvedges was then counted across a present outcrop width of 7.9 m measured perpendicular to the cleavage. The total width of the selvedges (a range of 35.4–54 cm) was then multiplied by 2.8, a factor representing the dissolved material, to give an estimate of the original width now represented by the cleavages (99–152 cm). The original width of the present 7.9 m width was then estimated to be 8.8–9.5 cm. Shortening was then calculated to be in the range of 11–16%. Although this range overlaps the shortening value determined from the micrite bed, the shale value is less accurate because the error in estimating the thickness and number of the cleavage selvedges is larger than it is in the micrite bed.

It is concluded that the formation of the cleavage and consequent shortening in the shale occurred during imbricate faulting in the micrite bed. Because it has already been proven that the faults represent a time-transgressive sequence that developed from east to west, it must also be concluded that the cleavage in the surrounding shales developed in a similar manner. The time-transgressive nature of the cleavage would not be obvious, however, if the micrite bed and its faulted geometry were absent from the outcrop.

The next problem is the origin of S_r, the rotated cleavage, and S_t, the finely-spaced cleavage below the floor thrust. Because S_r is simply the rotated equivalent of S_1, it had to form during simple shear displacement on the floor and roof faults (Fig. 4a). Measurements of cleavage rotation taken at eight locations below the micrite bed averaged 36° whereas similar measurements taken at seven locations above the micrite bed averaged 27° (Table 1). These line rotations correspond to angular shear strains of 51° for the floor thrust and 33° for the various roof thrusts using equation (2.3) of Ramsay & Huber (1983) in which γ, the shear strain, equals:

Table 1. Strain data for shales adjacent to micrite bed

	S_1 Cleavage rotation			
	Line rotation		Average shear strain	
	Average (°)	Range (°)	Average (°)	Range (°)
Above micrite bed $n = 7$	27	11–36	33	20–50
Below micrite bed $n = 8$	36	24–46	51	31–60

	S_t Cleavage			
	θ Observed		θ Calculated	
	Average (°)	Range (°)	Average (°)	Range (°)
Above micrite bed $n = 6$	32	16–40	37	31–40
Below micrite bed $n = 8$	21	13–28	29	24–36

$$\gamma = \cot \alpha - \cot \alpha'. \quad (1)$$

In this equation α and α' are the angles of S_1 and S_r, respectively, from the fault surface. The fact that S_r below the thrust has been rotated in most cases through a greater angle than S_r above the thrust is consistent with an earlier conclusion that the floor thrust was active throughout deformation whereas the individual roof faults were only active during the time interval between the formation of adjacent imbricate faults.

The S_t cleavage cuts across S_r at a low angle and is not folded or rotated near any of the faults (Figs. 3a and 4a). Although S_t is best developed below the floor thrust, it is also present just above the roof thrusts where the cleavage is less distinct and occupies a thin zone. Because S_t is confined to a narrow zone near the faults, it most likely developed as a result of simple shear which rotated the S_1 cleavage. In order to test this hypothesis the angle between S_t and the nearby fault, θ', was measured and compared with a calculated value predicted by the Ramsay equation (Ramsay & Huber 1983, equation 2.4)

$$\tan 2\theta' = 2/\gamma. \quad (2)$$

The values of γ were calculated from the rotation of the cleavage using the equation described in the foregoing paragraph (Ramsay & Huber 1983, equation 2.3). This equation predicts the acute angle, θ', between the plane defined by λ_1 and λ_2 of the strain ellipsoid and the plane of simple shear which in this case is the fault surface. In the ideal case of simple shear S_t will be parallel to the $\lambda_1 - \lambda_2$ principal plane of the strain ellipsoid. Thus the calculated and observed values should be the same within the margin of error providing no mechanism other than simple shear was involved. Along the floor fault the calculated angle between S_t and the fault is an average of 29° for eight separate locations (Table 1). The observed value, however, was an average of 21°. Along the higher roof thrust the calculated angle between S_t and the nearby fault was an average of 37° for six locations whereas the observed value was 32°.

Although the sample population is small and the corresponding standard deviations large for both the calculated and observed values, the differences do suggest two important relations. First, the angle θ' between S_t and the fault is larger along the roof thrust than it is for the floor thrust (Table 1). This relation simply reflects the smaller shear strain along the roof thrust compared to the floor thrust. Second, and more importantly, the calculated angle θ' between S_t and the nearby faults is consistently larger than the observed angle by values that range from 8° for the floor thrust to 5° for the roof thrust (Table 1). This relation is important because it suggests either that the S_t cleavage has been subsequently flattened by some sort of vertical loading after simple shear or that volume reduction, which has occurred during the formation of S_t, has indeed reduced the θ' angle.

In order to evaluate this problem further, calculations were made by Jean Crespi (written communication, 1989) using equations from Ramsay & Huber (1983, equations B.14, B.21 and D.13) involving volume reduction and simple shear. These calculations were then tested by the author on a Macintosh Computer using the drawing tools of Adobe Illustrator software. In the first model, the volume across the fault zone was reduced by an arbitrary amount and then subjected to simple shear so as to produce as closely as possible the angular relations of S_r and S_t below the micrite bed. In the second model, an assumed volume reduction was eliminated and then the resulting simple shear calculated using the line rotation needed to return S_r back to its unrotated state, S_1. Although our analysis requires further study, it does suggest that a volume reduction in the range of 25–30% could produce the $S_r - S_t$ geometry in the fault zone. Furthermore, the analysis indicates that the amount of simple shear calculated directly from the line rotation between S_1 and S_r (Table 1) will always be too large when other processes such as volume reduction or pure shear are involved. The volume reduction models cited above are still not realistic since S_t probably formed during the rotation of S_1. The fact that S_t cuts across the rotated S_1 cleavage must mean that the form and position of S_t continually changed during simple shear and volume reduction. In fact, the simple shear calculations (equations 1 and 2) assume this to be the case.

Are S_r and S_t time transgressive to the west? Because I have demonstrated earlier that the floor fault and the respective roof faults are time transgressive, it must follow that both S_r and S_t are also time transgressive. This conclusion suggests that the amount of rotation of S_r and the intensity of S_t should also increase to the east, particularly along the floor thrust where the displacement is larger and has taken place over a longer period of time. Although these cleavages were evaluated across the outcrop, I could not detect within the error of my measurements any such relation for S_r or S_t. This observation suggests that the mechanical process of bending the S_1 cleavage may become more difficult as the line rotation approaches 35° during simple shear and other deformational mechanisms progressively take over. Possible mechanisms include fault slip and/or the continued development of the S_t cleavage. Sorting out the various strain processes and deformational mechanisms along fault zones is a complicated matter and requires more study than is within the scope of this paper.

EVOLUTION OF STRUCTURES

The evolution of the imbricate faults and the various cleavages described in the foregoing section is illustrated in a series of retrodeformed sections in Fig. 6. Section 1 shows the outcrop at South Hero in its present state. Section 2 is developed by reversing the deformation associated with the youngest ramp fault at the western part of the outcrop. The remaining four sections are formed by systematically unfaulting the micrite bed from west to east in the reverse order of their formation. For example, in section 2 the hangingwall block (B, section 2) is unfolded as it is returned to its original position east of the footwall block (A, section 2). During this time the active fault which carried the eastern sequence westward was the floor thrust below segments D and E, the ramp fault just below segment C, and the roof thrust above segments B and A, which were then undeformed. In the shale above and below this active fault the S_1 cleavage is shown in a flatter position (S_r) as a result of rotation generated by east-over-west simple shear. Note that the rotated cleavage, S_r, is absent below blocks A and B since, at this time, the micrite bed is attached to the underlying shale. The fault-zone cleavage, S_t, is also shown in the shale along the active fault. I believe that this cleavage developed during the evolution of the imbricate structures, rather than after all the imbricate faults had formed, because S_t is present, although poorly developed, along the roof thrust above each segment of the micrite bed. If the fault-zone cleavage had formed after all the imbricate faults had moved into place, then it (S_t) would only be found along the floor thrust. The S_t cleavage therefore must have developed during the formation of each imbricate fault.

As a consequence of reversing the displacement on the fault and unfolding the ramp fold, the volume in the adjacent shale must be increased by eliminating much of the cleavage below segments A and B of the micrite bed. Note, however, that the density of S_1 cleavage in the thrust plate above segments A and B is essentially the same across section 2. This diagram is drawn in this way because I believe that the upper plate of the active fault was probably being shortened as a result of ramps or irregularities along the fault surface farther to the west. In actual fact, however, the density of S_1 in the upper plate must decrease to the west because, first, this is what is observed to the west across South Hero Island and, second, the overall stress intensity during deformation in theoretical models diminishes from the hinterland to the foreland (for example, Hubbert 1951, Chapple 1979, Davis *et al.* 1983). Thus, at any one time the

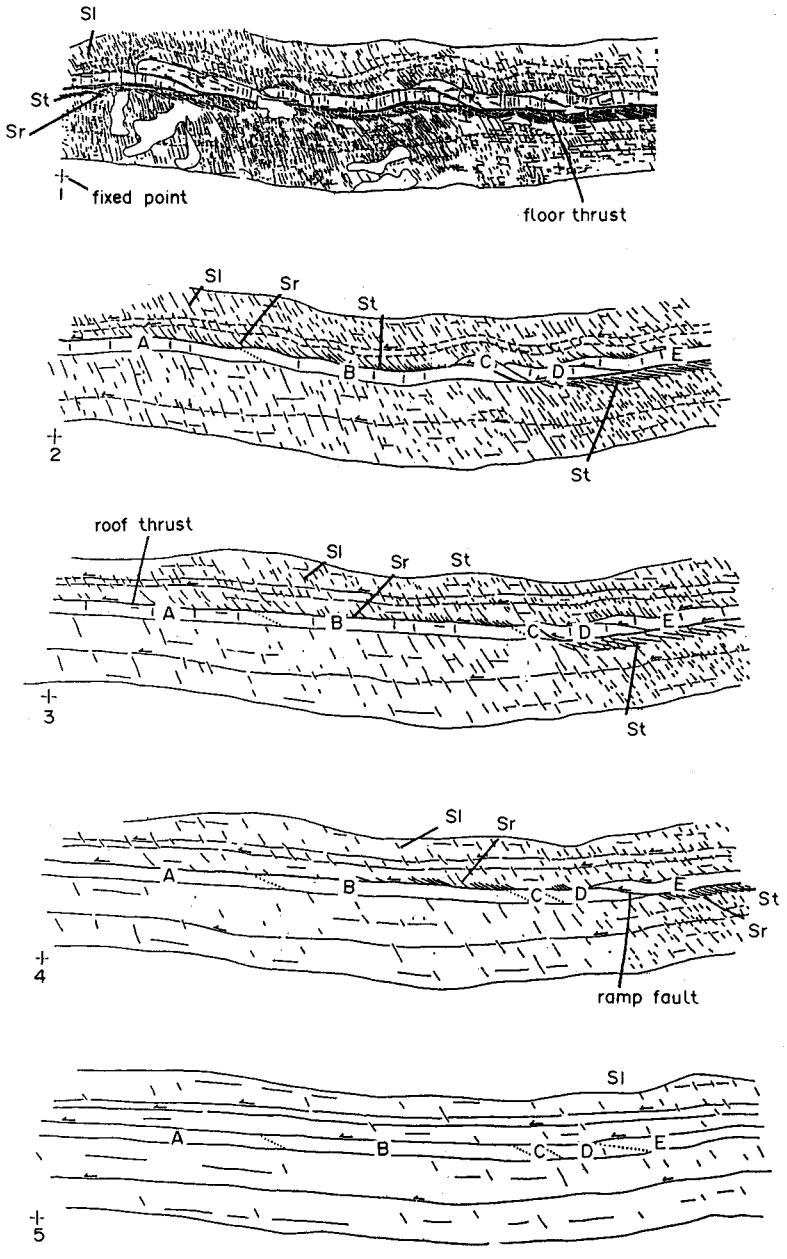

Fig. 6. The evolution of structures in the micrite bed ('beam') and surrounding shales of the Cumberland Head Formation. Section 1 is the outcrop in its present-day form. Sections 2–5 represent successive stages of retrodeformation in which the deformation is reversed beginning with the youngest imbricate thrust at the west end of the outcrop and ending with the oldest imbricate thrust on the east end of the outcrop. The evolution can then be seen by going from section 5 to section 1. The symbols are explained in Fig. 2.

cleavage density not only diminishes toward the foreland but it also changes in the same way from the upper plate to the lower plate (compare sections 2–5). As deformation progresses, older cleavage surfaces continue to grow in thickness and vertical extent and younger surfaces nucleate in older microlithons and grow essentially parallel to the older S_1 surfaces. In the end, the S_1 cleavage is uniformly developed across the outcrop and appears to the casual observer to be coeval because its style and orientation are the same. As can be seen in these series of sections, however, the S_1 cleavage is clearly a time transgressive structure.

Sections 3–5 show the retrodeformation continuing to the east and are constructed in the same manner as section 2. Thus the evolution of the imbricate system and its associated structures can be seen by studying diagrams 5–1. Clearly all the structures are time transgressive from east to west as they are traced through section 5 to section 1. During deformation the floor thrust or basal décollement undergoes repeated W-directed movement. As a result the S_r cleavage is rotated farther along the floor thrust than it is along the roof thrusts. When this angle reaches values in the range of 30–35°, it appears that other mechanisms such as fault slip or the continued development of the S_t cleavage takes over in the deformational sequence. Because the floor thrust continually moves, the S_t cleavage is better developed there than along any of the other faults.

DISCUSSION—FLUIDS, PORE PRESSURE AND DEFORMATION RATES

The presence of abundant calcite veins in the micrite bed and calcite-rich sills along all the faults throughout the outcrop indicates that fluids rich in CaO, CO_2, SiO_2 and H_2O were present during deformation. This fluid, which was present most likely as an interstitial fluid in the surrounding shale, became enriched in calcite and quartz due to pressure solution. Although these fluids could have come from a source external to the outcrop at South Hero, it is far more likely that they were locally derived. Furthermore, it is also clear that deformation was relatively rapid during the development of the fractures and faults since all the deposits contain only sparry calcite. In the shale, however, the rate of deformation was slow because it was controlled by the rate of dissolution of calcite and transport of the resulting fluid during the deformation of the pressure-solution cleavages. Movement of fluids in the shale between fracture events was probably slow because the permeability and porosity was low. Thus the nature of the rock and character of the calcite in the veins are strong evidence that deformation at South Hero occurred at two different rates.

The next important question to evaluate is whether abnormal pore pressures existed during deformation. Pore pressures greater than the hydrostatic value (0.45 of the total overburden pressure) can occur where the rate of increase in the pore pressure is greater than the rate at which the fluids or gases can leak out to the surface (Rubey & Hubbert 1959). This can happen when a rock sequence is vertically loaded either by rapid sedimentation, or by tectonic compression that results in rapid movement on imbricate faults, as described in an excellent paper by Gretener (1972). At South Hero an added tectonic load was developed at each of the ramp areas when the hangingwall overrode the footwall. We know that this movement was rapid because all the fractures associated with the faults are filled with sparry calcite. It is therefore likely that abnormal pore pressure developed in this area. The abundant calcite veins and clastic dikes in some of the ramp areas supports this suggestion (Fig. 4d). Furthermore, it is quite likely that pore pressure may have also increased in the surrounding shales during this time since they too were rapidly loaded as the beam suddenly failed. These pressures lasted in the ramp region until the hangingwall rocks were sufficiently fractured that the rate of fluid transfer out of the system was greater than the rate of fluid pressure increase. The time interval of abnormal pressure was short since the hangingwall block had to be deformed by fracturing and movement on older planes of weakness in order to adjust to the fold geometry in the ramp region. The abnormal pressure for this outcrop at South Hero can be estimated from a knowledge of the thickness of the overlying rock during deformation and the value of rock density. If we assume no additional tectonic load, the vertical pressure is calculated to be 0.25 kb (250 Pa) using an estimated density of 2.4×10^3 kg m^{-3} for lithified shale and micrite (Turcotte & Schubert 1982) and an undeformed stratigraphic thickness of 1065 m (3500 ft) taken from Welby (1961). Thus the hydrostatic pressure would be 0.11 kb (113 Pa) assuming that it is 0.45 of the pressure of the saturated rock. Any value of pore pressure greater than 0.11 kb would be considered abnormal. All these values, however, should probably be increased accordingly since it is likely that deformation at the 'beam' did involve a tectonically thickened section due to faulting farther to the east (Causeway thrust fault, for example, Fig. 2a).

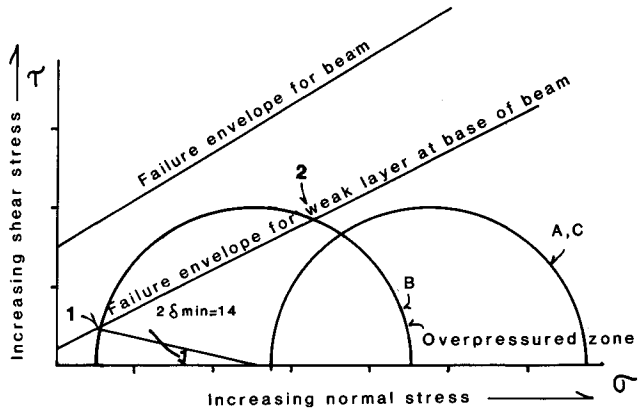

Fig. 7. Mohr diagram showing the failure envelope for the weak layer (floor fault or basal décollement) and the strong layer (the 'beam'). The half Mohr circle labelled 'A, C' represents a hypothetical state of differential stress under normal hydrostatic pressure whereas the Mohr circle labelled 'B' represents the same differential stress state but under conditions of abnormal pressure. The angle labelled '$2\delta_{min} = 14°$' represents the orientation of the weak layer relative to the direction of σ_1. The figure was taken from Gretener (1972).

What affect then did the abnormal pore pressure have upon subsequent faulting? It is well established that abnormal pore pressure reduces the frictional resistance along potential or pre-existing faults by reducing the effective normal stress across these surfaces (Hubbert & Rubey 1959, Handin *et al.* 1963, for example). Thus with increasing pore pressure the frictional resistance along a fault is reduced and movement can therefore occur at lower differential stress. This relation is nicely shown on a Mohr–Coulomb diagram taken from Gretener (1972). In Fig. 7 two states of stress in a rock sequence such as seen at the outcrop at South Hero are represented by the two half Mohr circles. Since the differential stress for both these states is the same their location on the Mohr diagram is a function of the difference in pore pressure between states A and C, which is considered by Gretener (1972) to be at hydrostatic pressure, and state B, which is overpressured. According to the foregoing discussion the overpressured zone at South Hero would have most likely existed along the base of the micrite bed in the ramp region (Figs. 3a and 4d, for example). The abundance of calcite deposits in this zone certainly supports this inference. States A–C would then represent the stress condition in the shale beneath the 'beam' and in the rocks of the hangingwall above the ramp fault.

The following scenario is then presented. As frictional resistance was increasing due to bending of the hanging-

wall block during movement on the ramp fault, the abnormal pore pressure along the base of the micrite bed on the footwall affectively weakened the rock so that subsequent shortening was transferred to this bedding plane. As a result the floor thrust which was active to the east of the ramp, propagated westward beneath the active ramp. At this time movement essentially ceased on the ramp and the overlying roof faults, which had just been active. Eventually the new westward extension of the floor fault cut across the micrite beam on a younger ramp fault to the west and the whole process, which has just been described, was repeated.

The concept of a plane of superweakness discussed by Gretener (1972) can also be applied to the outcrop at South Hero. As shown on Fig. 7 the upper line represents the failure envelope for the micrite bed whereas the lower line represents the envelope for the relatively weak bedding planes between the micrite bed and the surrounding shale. Both layers have an inherent cohesive strength represented by the respective intercepts on the τ axis. As the pore pressure increased along the base of the micrite layer during movement on the ramp fault, the state of stress represented by half circle A–C moved left to position B. As shown in this figure, failure occurs at point 1 rather than at some other point between 1 and 2 because σ_1 is oriented 7° from the weak bedding plane according to Gretener's figure. Fortuitously, this value is in fairly close agreement with the early extension fractures at the South Hero outcrop. Here the angle between the extension fractures in the early W-climbing arrays and the nearby bedding varies between 7 and 11° (Figs. 4a–c). This relation indicates that σ_1 had to be inclined to bedding in such a way that east-over-west shear could develop along bedding. Furthermore, the presence of older bedding plane thrusts (T_0), which are cut by the S_1 cleavage in the surrounding shales, indicates that σ_1 was in this position even before the extension fractures had developed in the micrite bed. Thus failure along the weak layer at the base of the micrite bed beneath the active ramp is facilitated by the increase in pore pressure resulting from rapid tectonic loading. As a result of this process taking place at each of the ramp areas, active displacement is continually transferred from the ramp and roof faults to the floor fault.

I have discussed arguments supporting alternating periods of rapid and slow displacement during the compression of the rock sequence at South Hero. I believe that the compressive load is cyclically transferred from the micrite bed to the shale and back again as the shortening mechanism changes from fault development to cleavage formation. Gretener (1972, fig. 15) illustrates this type of cyclical deformation with the Mohr diagram. Figure 8 is very similar to Fig. 7 except here the larger Mohr circles represent progressively increasing state of differential stress with the larger ones to the right representing the stress state in the micrite bed (beam) and the smaller ones to the left representing the stress states in the surrounding shales. When the sequence was first subjected to compression the load was largely supported by the micrite bed. The increase in the compressive stress is represented by the progressively larger Mohr circles in which the left intercept on the σ axis represents the effective confining pressure, which is approximately 0.14 kb for South Hero if we used an undeformed stratigraphic thickness of 1065 m cited earlier. Failure along a ramp fault occurred when the largest Mohr circle on Fig. 8 was tangent to the failure envelope for the beam. When this occurred the differential stress in the beam rapidly decreased and the load was then transferred to the surrounding shales. As a result, the Mohr circle for the beam became smaller and the corresponding circle for the shale became larger as the differential stress built up due to increasing compressive load. However, the development of the Mohr circle for the shale was quite different than it was for the beam. Instead of the left intercept, which represents the effec-

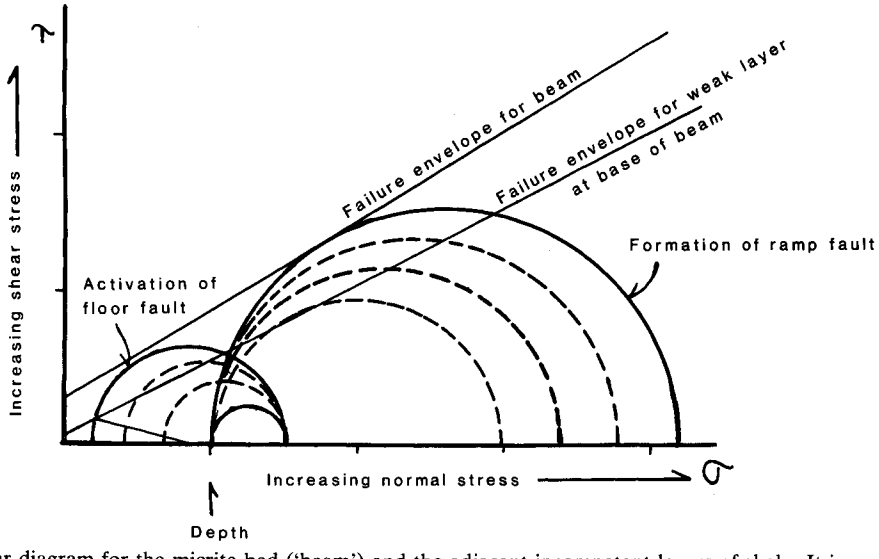

Fig. 8. Mohr diagram for the micrite bed ('beam') and the adjacent incompetent layers of shale. It is assumed that the vertical stress is essentially the same in both rock types. The larger Mohr circles represent the increasing load in the beam. The smaller Mohr circles represent the increasing differential stress in the shale after the beam fails along the ramp fault.

tive load pressure in the shale and beam, remaining fixed as it did when the differential stress built up in the beam, it now moves to the left. The reason for this difference is the sudden increase in pore pressure that had developed from the rapid increase in tectonic load beneath the active ramp. As a result the effective confining pressure (left intercept) decreased. The axial load, which is the right intercept on the σ axis, remained constant according to Gretener's original figure (1972, fig. 15) because the increase in compressive load, which has been transferred from the beam, was offset by the increase in pore pressure. In essence the pore fluids temporarily supported the added horizontal compression. With the continued increase in pore pressure the frictional resistance along the basal bedding plane (the weak layer) of the beam beneath the active ramp decreased until it failed and the floor thrust was formed (left-most Mohr circle on Fig. 8). When new fractures developed in the hangingwall block and in the ramp area the pore pressure gradually decreased. Eventually, the basal plane failed forming the floor fault. In order for the floor fault to continue to propagate to the west of an active ramp, it is likely that a pocket of abnormal pore pressure advanced as a wave or edge dislocation. Perhaps these levels are maintained by the continual dissolution of calcite during cleavage formation in the surrounding shales. Certainly the numerous dikes and sills of calcite along the floor thrust indicated repeated intrusion of fluids during faulting. Eventually, however, the differential stress was transferred back to the beam as the frictional resistance along the floor fault increased and pressure solution had accounted for all the required shortening in the shale section. As the load was again transferred back to the beam the differential stress built up and the corresponding Mohr circles would again expand to the right (Fig. 8). Thus the cycle was repeated during the formation of the next ramp to the west. The sequence of events described by Gretener (1972) therefore is directly applicable to the evolution of the imbricate structures at South Hero. The beauty of outcrops such as this is that the evidence for their evolution and processes of development can be seen directly at the outcrop and need not be inferred from fragmentary geometrical information.

CONCLUSIONS

Although the conclusions reached in this study are directly applicable to outcrop-scale features in sequences of thinly bedded shale and limestone, they do provide insight into the processes and mechanics involved with larger structures of the foreland whose geometry is not directly accessible. Extrapolation to these larger structures, however, must be done with care so that the relative thicknesses and difference in the mechanical properties of the rock sequence are directly proportional to the change in scale of the structure. The following list summarizes the important conclusions.

(1) Ramp faults developed from W-climbing, en échelon arrays of extension fractures. The early arrays were deformed by east-over-west shear and were superposed by younger W-climbing arrays. These events so weaken the zone that eventually a through-going ramp fault developed.

(2) The imbricate faults progressively developed toward the foreland. The floor thrust or décollement at the base of the micrite bed was reactivated throughout deformation whereas each of the ramp faults and overlying roof thrust were sequentially deactivated as the system progresses to the west.

(3) Fracture and fault events were relatively rapid as evidenced by the presence of sparry calcite within and along these features.

(4) The thickness of the calcite deposits along a fault is directly proportional to length of time during which a fault was active. These deposits formed by repeated injection of calcite rich fluids and were subsequently deformed by pressure solution along clay-rich selvedges which are interlayered with the calcite. This deformation forms the prominent slickenlines which characterize each of these layers.

(5) Simple shear (angle of shear of about 51°) and volume reduction (25–30%) along the floor and roof faults rotated the older S_1 cleavage and generated a younger, finely spaced, thrust-zone cleavage. This shear strain translates into approximately 60 cm of displacement on the basal décollement which represents an additional 36% to the displacement accommodated by folds and faults within and around the micrite bed.

(6) The shortening generated by faulting in the micrite bed (beam) was accommodated by the formation of pressure-solution cleavage in the shales. The development of cleavage was time transgressive from the hinterland to the foreland. During its evolution at any one place the individual cleavage surfaces became thicker, more abundant and more extensive.

(7) Shortening in the shales by cleavage took place slowly and was a function of the rate at which the dissolved material could be transported out of the shale. Thus deformation alternated from fast to slow as the compressive load was transferred from the beam to the shale as the structures progressively developed toward the west.

(8) Abnormal pore pressures most likely existed beneath the active ramp areas. This condition moved westward as the floor fault propagated toward the foreland.

Acknowledgements—Many students in my course, entitled "Structural Analysis of Deformed Rocks", at the University of Vermont have studied and contributed to my understanding of the 'beam'. I acknowledge their stimulation and enthusiasm. Katherine Leonard studied the fault zone as part of her M.Sc. degree. Discussions with Jean Crespi of Brown University (U.S.A.) were particularly stimulating. Her thoughts and calculations on volume reduction along the floor thrust were very helpful. Peer reviews by two anonymous geologists added clarity and conciseness to the paper.

REFERENCES

Bosworth, W. 1983. Foreland deformation in the Appalachian Plateau, central New York: the role of small-scale detachment structures in regional overthrusting. *J. Struct. Geol.* **6**, 73–81.

Boyer, S. E. & Elliot, D. 1982. Thrust systems. *Bull. Am. Ass. Petrol. Geol.* **66**, 1196–1230.

Chapple, W. M. 1978. Mechanics of thin-skinned fold-and-thrust belts. *Bull. geol. Soc. Am.* **89**, 1189–1198.

Davis, D., Suppe, J. & Dahlen, F. A. 1983. Mechanics of fold and thrust belts and accretionary wedges. *J. geophys. Res.* **88**, 1153–1172.

Dorsey, R. L., Agnew, P. C., Carter, C. M., Rosencrantz, E. J. & Stanley, R. S. 1983. Bedrock geology of the Milton quadrangle, northwestern Vermont. *Vermont geol. Surv., Spec. Bull.* **3**.

Doll, C. G., Cady, W. M., Thompson, J. B. Jr & Billings, M. P. 1961. Centennial Geologic Map of Vermont. Montpelier, Vermont. *Vermont Geol. Surv.* Scale 1 : 250,000.

Gretener, P. E. 1972. Thoughts on overthrust faulting in a layered sequence. *Bull. Can. Petrol. Geol.* **20**, 583–607.

Gwinn, V. E. 1970. Kinematic patterns and estimates of crustal shortening. In: *Studies in Appalachian Geology—Central and Southern* (edited by Fisher, G. W., Pettijohn, F. J., Reed, J. C., Jr & Weaver, K. N.). Interscience, New York, 127–147.

Handin, J., Hager, R. V., Friedman, M. & Feather, J. N. 1963. Experimental deformation of sedimentary rocks under confining pressure: pore pressure tests. *Bull. Am. Ass. Petrol. Geol.* **47**, 717–755.

Hubbert, M. K. 1951. Mechanical basis for certain familiar geological structures. *Bull. geol. Soc. Am.* **62**, 365–372.

Hubbert, M. K. & Rubey, W. W. 1959. Role of fluid pressure in mechanics of overthrust faulting. *Bull. geol. Soc. Am.* **70**, 115–166.

Leonard, K. E. 1985. Foreland fold and thrust belt deformation chronology, Ordovician limestone and shale, Northwestern Vermont. Unpublished M.Sc. thesis, University of Vermont, Burlington, Vermont.

Nickelson, R. P. 1986. Cleavage duplexes in the Marcellus Shale of the Appalachian foreland. *J. Struct. Geol.* **8**, 361–372.

Rowley, D. B. 1982. New methods for estimating displacements of thrust faults affecting Atlantic-type margins; with applications to the Champlain thrust, Vermont. *Tectonics* **1**, 369–388.

Ramsay, J. G. & Huber, M. I. 1983. *The Techniques of Modern Structural Geology, Volume* 1: *Strain Analysis*. Academic Press, London.

Ramsay, J. G. & Huber, M. I. 1987. *The Techniques of Modern Structural Geology, Volume* 2: *Folds and Fractures*. Academic Press, London, 309–700.

Rubey, W. W. & Hubert, M. K. 1959. Role of fluid pressure in mechanics of overthrust faulting: II. Overthrust belt in geosynclinal area of western Wyoming in light of fluid-pressure hypothesis. *Bull. geol. Soc. Am.* **70**, 167–206.

Serra, S. 1977. *Wyoming Geological Association Guidebook 29th Annual Field Conference*, Jackson, Wyoming, 487–498.

Stanley, R. S. & Ratcliffe, N. M. 1985. Tectonic synthesis of the Taconian orogeny in western New England. *Bull. geol. Soc. Am.* **96**, 1227–1250.

Suppe, J. 1982. Geometry and kinematics of fault-related parallel folding. *Am. J. Sci.* **282**, 684–721.

Suppe, J. 1985. *Principles of Structural Geology*. Prentice-Hall, Englewood Cliffs, New Jersey.

Turcotte, D. L. & Schubert, G. 1982. *Geodynamics: Applications of Continuous Physics to Geological Problems*. John Wiley & Sons, New York.

Welby, C. W. 1961. Bedrock geology of the Champlain Valley of Vermont. *Vermont geol. Surv. Bull.* **14**.